Upgrade of a 32 m Small-angle Neutron Scattering Instrument, SANS-U

Satoshi Okabe, Michihiro Nagao, Takeshi Karino,* Satoshi Watanabe, and Mitsuhiro Shibayama†
Neutron Science Laboratory, Institute for Solid State Physics,
The University of Tokyo, Tokai, Ibaraki 319-1106, Japan
CREST, Japan Science and Technology Agency,
4-1-8 Honcho Kawaguchi, Saitama 332-0012, Japan
(Dated: January 25, 2006)

The small-angle neutron scattering instrument, SANS-U, owned by the Institute for Solid State Physics (ISSP), The University of Tokyo, has been upgraded. The SANS-U is a 32 m-SANS instrument installed in 1991 at the guide hall of the JRR-3M research reactor of the Japan Atomic Energy Research Institute (JAERI), and has been served as an inter-university cooperative research use since 1993. The major upgrades are (1) a replacement of the two-dimensional area detector from a single-wire type position-sensitive proportional counter to a multi-wire type, (2) a renewal of the operating system from a VAX and sequencers to an integrated PXI system controlled by LabVIEW-RT software, (3) a focusing collimation system, and (4) a variety of accessory equipments, such as furnace, high pressure cell, shear cell, in addition to a versatile sample changer. These upgrades provide a wide dynamic range of neutron counting, user-friendly operation, and real-time circular averaging of the two-dimensional data.

I. INTRODUCTION

Small-angle neutron scattering (SANS) is a unique and non-destructive method for structural analyses in many fields, such as biological and polymeric systems, colloidal suspensions, membranes, flux lines in superconductors, etc. The structural information obtained by SANS covers the spatial range of a few to hundred nanometer and have been revealing important scientific findings for more than three decades.(Higgins, 1994; Schelten, 1974) Because of the above usefulness, a large number of steady reactor-sourced SANS instruments have been constructed and served for users, e.g., D11 (1972 -) and D22 (1995 -) at ILL, NG1, NG3 (1992 -), and NG7 (1991 -) at NIST (Glinka, 1998), SANS-J (JAERI, Tokai), and SANS-U (ISSP, Tokai) (Ito, 1995), etc., in addition to pulsed neutron-sourced instruments, such as, LOQ at ISIS (Heenan, 1997), SASI & SAND at IPNS, LQD at LANSCE, SWAN at KEK (Otomo, 1999). New powerful SANS instruments are under construction at ORNL (U. S. A.), HANARO (Korea), ANSTO (Australia), etc.

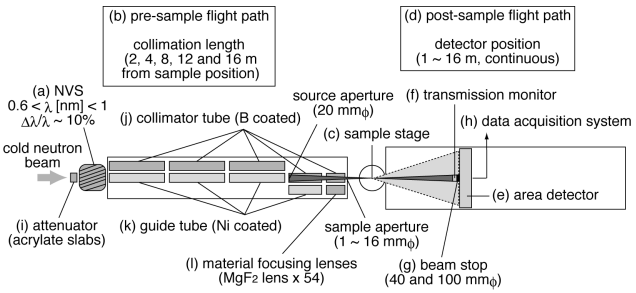

FIG. 1: The overview of the SANS-U.

The SANS-U, owned by the Institute for Solid State Physics, The University of Tokyo, was constructed in the guide hall of the 20 MW research reactor, JRR-3M, of the Japan Atomic Energy Research Institute (JAERI) in 1991 (Ito, 1995). Figure 1 shows the overview of SANS-U. This instrument is composed of (a) a mechanical neutron velocity selector (NVS), (b) a pre-sample flight path, (c) a multi purpose sample stage, (d) an evacuated post-sample flight path, (e) an area detector, (f) a point detector for transmission measurements, (g) a beam stop made of B_4C, and (h) a data acquisition system. The incident neutron beam from the cold source (white beam flux $\sim 2 \times 10^8$ cm^{-2}s^{-1} with the peak wavelength of 0.4 nm) is monochromatized by a NVS with helical slits (ASTRIUM, Germany) (Friedrich, 1989). Cold neutron beam from the reactor was guided to the NVS. If necessary, the beam can be attenuated by (i) polyacrylate slabs with different thicknesses (3, 5, and 7 mm). Just behind the NVS is located the pre-sample flight path, which consists of (j) pinhole tubes coated with B_4C inside and (k) alternate neutron guide tubes coated with Ni inside. By replacing the pinholes and the guide tubes in or out of the beam, users can change the effective source-to-sample distance (= collimation length, CL) to 1, 2, 4, 8, 12, or 16 m in order to vary the divergence and flux of the incident beam at the sample position. Normally, a symmetric optical arrangement, i.e., CL = SDD (sample-to-detector distance), is recommended to optimize the flux and divergence of the beam. The collimator apertures are 20 mmϕ each and the sample aperture can be chosen from 1, 3, 5, 7, 8, 10 to 16 mmϕ. (l) A set of material focusing lenses (Eskildsen, 1998; Choi, 2000), made of 54 pieces of MgF_2 biconcave lenses, can be inserted at the lower-most collimator tube position for converging optics. The focal length is 8.0 m for $\lambda = 0.70$ nm. The unique feature of the symmetric arrangement will be discussed later. For higher resolution experiments, CL is set to be longer than SDD. The sample stage is designed to be versatile for various types of sample systems. In the past decade, various types of sample sys-

*Also at CREST.
†Also at CREST.; Electronic address: sibayama@issp.u-tokyo.ac.jp

tems such as a high-pressure cell, a furnace, a shear cell, etc., have been developed by users and the Instrumentation and Research Team (IRT). Scattered neutrons are fed by an evacuated flight path, in which an area detector of 64.5 cm × 64.5 cm is installed on a truck running on rails to vary the SDD continuously from 1 m to 16 m. A slide-in type direct beam stop and beam monitor for measurements of transmission are mounted on the truck just in front of the detector.

The beam time of SANS-U is allocated to users whose proposals have passed through a review by the neutron scattering program advisory committee (NSPAC) of the Reactor Beam Users. For the purpose of instrumentation and special researches, about third of the whole beam time (175 days/y) is assigned to the IRT. The SANS-U accepts about 40 proposals/year from universities and governmental institutions and carries out SANS experiments. More than 20 research papers are published annually. However, due to chronic insufficiency of beam time, aging of the electronics and cables, and out-of dating of the computer systems, an upgrade of SANS-U had been highly demanded. In order to expand the applicable conditions of experiments and to improve the reliability, a major upgrade has been made by replacement of the area detector, the control system, and refurbishment of the cables, mechanical systems, electronic systems, etc. In this paper, we report the performance of the new SANS-U.

II. UPGRADE OF SANS-U

A. Replacement of the area detector

The two-dimensional area detector, which was a single-wired position sensitive proportional counter (PSPC; model 2650N, ORDELA, USA), was replaced by a multi-wired PSPC (model 2660N, ORDELA, USA). Because of the multi-wired cathodes for both the horizontal (X) and vertical (Y) directions and a lower ^{3}He gas pressure, the maximum count rate was raised from 10^5 to 10^6 cps/detector (catalogue base). For safety use, we regulate the upper limit of counting rate to be 7000 cps/detector and 200 cps/pixel. The data acquisition system (DAS100) was also supplied by ORDELA, which is an integrated board developed for data accumulation and detector configurations.

B. Replacement of the SANS-U control system

The previous SANS-U control system ran on a VAX with a set of sequencers. The experimental conditions were set by way of isolated sequencers. By upgrading, the SANS-U control system was replaced by a LabVIEW-RT system running on a PXI (PCI eXtensions for Instrumentation) system. The new SANS-U control system contains five WINDOWS and one Macintosh computers, the control panel, and the peripheral devices. Figure 2 shows the diagram of the relationship between the devices and the control system. (a) The

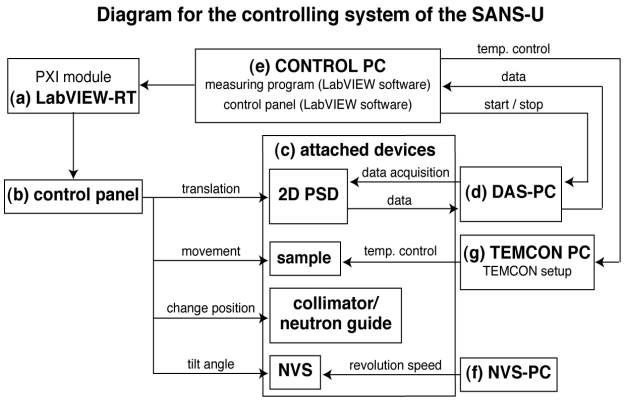

FIG. 2: Diagram of the SANS-U control system.

LabVIEW-RT is an operating system, which has good compatibility with LabVIEW applications and guarantees a long-run stability. The main liquid-crystal display of the SANS-U control system has a mirror image of (b) the control panel, which allows a remote control of the experiment from the computer. All of the commands, such as change of collimation, sample change, goniometer control, temperature control, can be sent to (c) the peripheral devices. The scattering intensity data collected by the area detector was transferred to (d) the DAS-PC, followed by (e) the control PC. The NVS is controlled by (f) NVS-PC. A temperature control device (TEMCON) is operated by (g) TEMCON-PC (Noda, 1983). Since the SANS-U control program is written in LabVIEW, the system is very versatile and provides an amenity operation.

C. Real time circular/sectorial averaging

The LabVIEW environment also realizes easy integration of data acquisition and primitive analyses. The control system installed at the SANS-U contains a real time circular averaging function, which converts an original two-dimensional scattering intensity pattern to a circularly averaged one-dimensional profile. By simply typing the center channel of the profile and the rate of re-flushing, users are able to watch the evolution of the scattering profile during measurement. The resulting one-dimensional data and the original two-dimensional data are stored automatically to the control PC. Users are allowed to transfer the data to their own computers any time. This function has drastically improved operating efficiency as well as capability of designing the experiment *in situ*.

D. Accessories

A 500 mmϕ diameter sample stage is located between the pre- and post-sample flight paths. A variety of sample systems can be mounted on this stage, such as an automatic sample changer, an inner cell-type

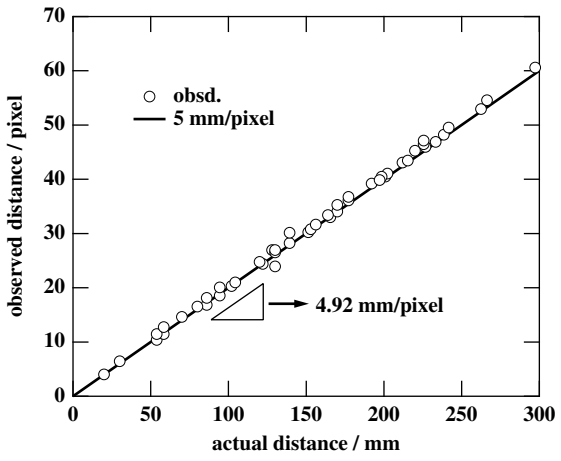

FIG. 3: The spatial linearity of the area detector of SANS-U.

high-pressure cell (HP cell), a shear cell with a thermometer covering the range of shear rate from 10^{-3} to 10^3 s^{-1} (Takahashi, 2000), a furnace for high temperature up to 250 °C, and a cryostat with electromagnets. The sample changer has horizontally-aligned 10 sample holders and the sample position can be changed automatically. The chamber is designed to tolerate evacuation for the use of high ($\leq$ 200°C) and low ($\geq$ 10°C) temperatures by either electric heater or water circulation. The HP cell has recently been designed to carry out high-pressure experiments for polymer solution or microemulsion systems. The accessible pressure is 400 MPa. Some experimental results have already been published (Shibayama, 2004; Nasimova, 2004ab). Though it is under establishment, the details of the HP cell will be reported elsewhere in the near future. The sample stage can be rotated for fine adjustment of the sample systems to the optic axis and especially for θ-scan of solid-state crystals. Except for the shear cell system, the temperature of the sample can be controlled precisely by using TEMCON system (Noda, 1983) with an accuracy of less than 0.01 °C.

III. CALIBRATION AND PERFORMANCE

A. Linearity of the detector

The linearity of the detector was measured by carrying out SANS measurement of a polyethylene (PE) slab. Here, just in front of the detector was placed a cadmium plate with 3 mm diameter holes aligned 5 cm interval orthogonally. Figure 3 shows the observed distances (in pixel) of the apertures from the center channel of the detector against the actual distances (in mm) from the center of the detector plane. This clearly indicates that the positions of the apertures are detected properly, meaning good linearity of the detector with 1 pixel = 4.92 mm.

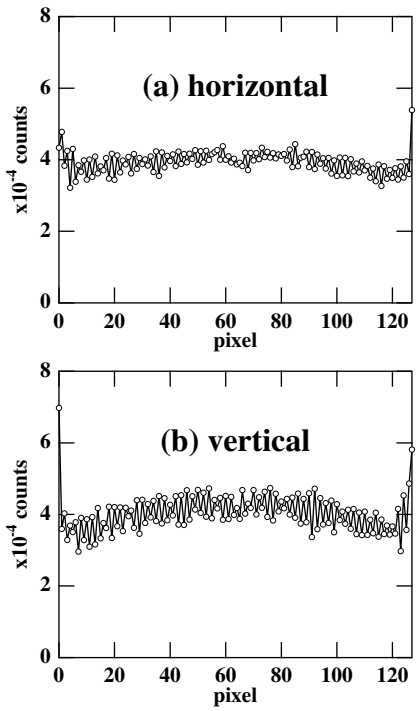

FIG. 4: Performance test of the detector uniformity. (a) Horizontally (x-axis) and (b) vertically (y-axis) integrated incoherent scattering profiles from a polyethylene standard sample.

B. Uniformity of the detector

The uniformity of the efficiency of the detector was measured by using incoherent scattering from H_2O in a quartz cell with the optical length of 2 mm. The scattering profile of H_2O was corrected for transmission, parasitic scattering from the cell and the dark current (Figure 4). The accumulated counts were 200 to 400 neutrons/pixels, resulting in 4×10^4 neutrons along the x- or y-directions. As shown in the figure, there are two types of inhomogeneities, i.e., odd-even type and gradient type inhomogeneities. Hence, currently we employ a pixel-to-pixel correction of the data by using incoherent scattering from a polyethylene secondary standard.

C. Center beam profile

Figure 5 shows the geometrical scheme of the symmetric optical arrangement for the cases of CL = SDD = 4 (dashed lines) and 8 m (solid lines). A 5 mmϕ sample aperture is also set in the beam line. As shown in the figure, the incident beam profile on the detector plane is uniquely determined independent of CL (and SDD). The full width at half maximum (FWHM) is calculated to be 4 pixels (= 19.7 mm) when a 5 mmϕ sample aperture is used. The center beam profile along the x-axis at the optics of SDD = CL = 4 m with λ = 0.70 nm is shown in Figure 6a. A similar profile was obtained

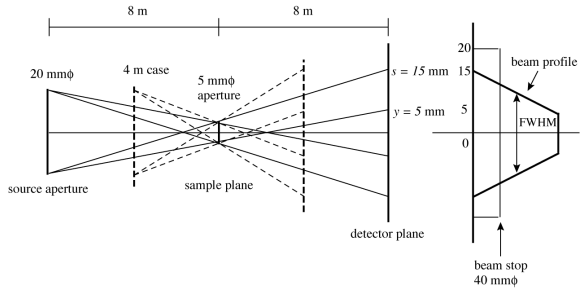

FIG. 5: The geometrical scheme of the symmetric arrangement of SANS-U for SDD = 8 (solid lines) and 4 m (dashed lines).

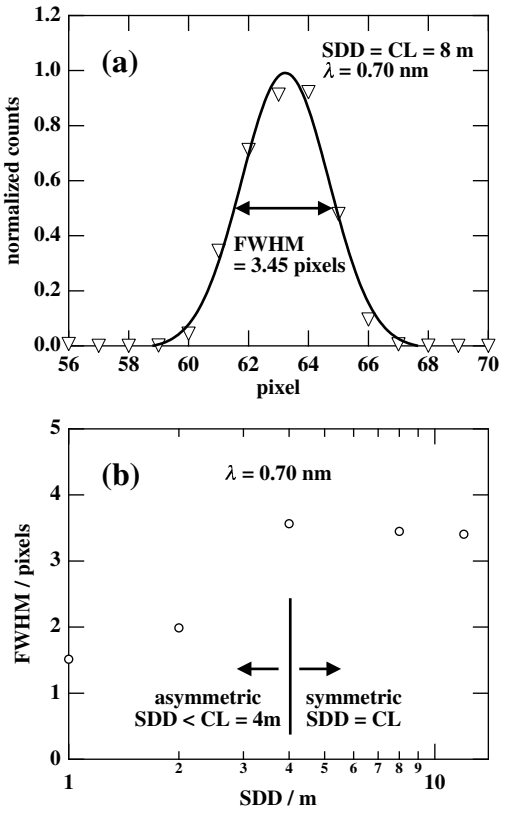

FIG. 6: (a) The center beam profile along the x-axis at SDD = CL = 8 m. (b) The SDD dependence of FWHM of the divergence of the center beam.

for the y-axis. The profile is nicely reproduced by a Gaussian function with FWHM of 3.45 pixels (= 17.3 mm), which is in good agreement with the evaluated value from Fig. 5. The FWHMs of the profile at other optical conditions are shown in Figure 6b. The value of FWHM increases with SDD up to 4m. This is due to the fact that CL was set to be constant, i.e., CL = 4 m, irrespective of SDD. On the other hand, a symmetrical optical condition was taken for the case with SDD $\geq$ 4 m. The neutron flux at the sample plane is 6.0×10^5 $\mathrm{cm}^{-2}\,\mathrm{sec}^{-1}$, in the case of CL = 4 m. The incident beam intensity at the detector plane, I^0_{det}, was found to be a

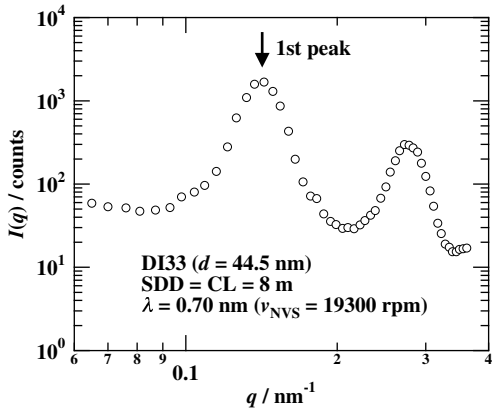

FIG. 7: The scattering intensity function from DI33 used for wavelength calibration. (SDD = CL = 8 m.)

function of SDD with a power of 1.91, $I^0_{\mathrm{det}} \propto \mathrm{SDD}^{-1.91}$ for the collimation-fixed optical conditions. The power ca. -2 is explained by the reduction of the solid angle covered by the detector plane with SDD. When the symmetric optical arrangement is applied, the relationship became $I^0_{\mathrm{det}} \propto \mathrm{SDD}^{-3.92}$. The additional power -2 with respect to the collimation-fixed case is due to the reduction of the effective source area determined by the end of the neutron guide with CL.

D. Wavelength calibration

The wavelength calibration is carried out using Bragg reflections from a microphase separated block copolymer film (poly(styrene-d_8)-poly(isoprene), sample code : DI33) at the beginning of each reactor cycle. Two-dimensional scattering patterns containing sharp peaks are obtained as a function of the NVS revolution speed, v_{NVS}. A sector averaging with 10° is carried out to obtain a scattering function shown in Figure 7. By using an assumed wavelength, λ_{assum}, the q-value of the first peak position, q_{assum}, is determined by curve fitting of the peak profile with a Gaussian function. Here, q is the magnitude of the scattering vector defined by $q = (4\pi/\lambda)\sin\theta$, where 2θ is the scattering angle and λ is the wavelength of the incident neutron beam. The Bragg spacing of the DI33, d, is known to be $d = 44.5$ nm determined by small-angle X-ray scattering (Matsushita, 1995). So the real wavelength, λ_{real}, can be obtained with the following equations.

$$q_{\mathrm{assum}}\lambda_{\mathrm{assum}} = q_{\mathrm{real}}\lambda_{\mathrm{real}} = \frac{2\pi}{d}\lambda_{\mathrm{real}} \qquad (1)$$

Usually, λ is selected to be 0.70 nm after iterating the above procedure at several v_{NVS} values by assuming a linear relationship between v_{NVS} and λ. Figure 8a shows the plot of the wavelength, λ, as a function of the v_{NVS}. As shown in the figure, the relationship is rather linear in this region. Figure 8b shows the λ dependence of the incident beam intensity, which is a

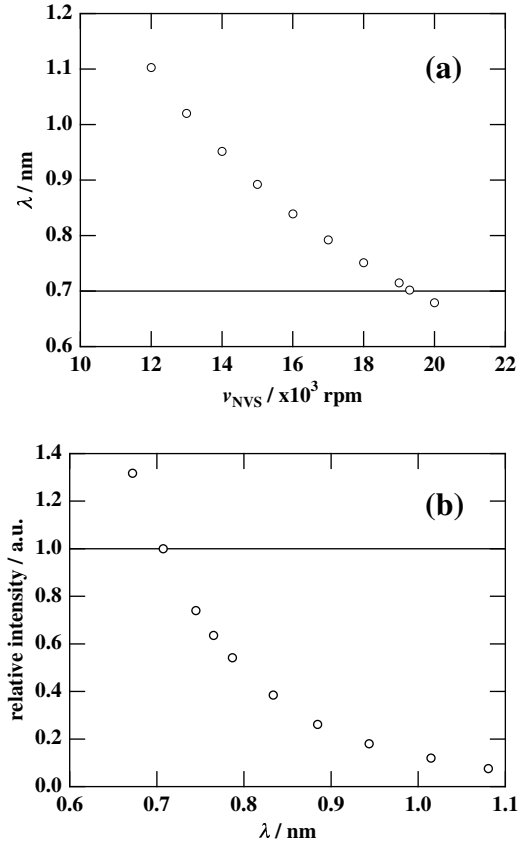

FIG. 8: (a) The NVS revolution speed, $v_{\rm NVS}$, dependence of the wavelength, λ, and (b) the λ-dependence of the relative incident beam intensity normalized at $\lambda = 0.7$ nm.

monotonically decreasing function of λ. From practical point of view, the wavelength $\lambda = 0.70$ nm is recommended by setting $v_{\rm NVS}$ around 1.90×10^4 rpm, which optimizes the flux and the q-resolution. The adjustable λ is $0.6 < q[\mathrm{nm}^{-1}] < 1.0$. The wavelength distribution is 10 % (FWHM) according to the manual of the NVS (Friedrich, 1989).

E. Accessible q-range

The accessible q-range was evaluated by measuring incoherent scattering from Lupolen at various optical conditions. The scattering profiles are shown in Figure 9 for the cases of (a) CL = 4 m, SDD = 1 m, (b) CL = 4 m, SDD = 2 m, (c) CL = 4 m, SDD = 4 m, (d) CL = 8 m, SDD = 8 m, and (e) CL = 12 m, SDD = 12 m. The valid q-range was evaluated from the flat range of the scattering intensity in the figure. At $q \leq 0.16$ nm^{-1}, a slight upturn due to the concentration fluctuation of polyethylene is observed. However, it does not affect to the accessible q-range of the spectrometer. For example, when SDD = 4 m and CL = 4 m with $\lambda = 0.70$ nm, the accessible q-range is $0.08 < q[\mathrm{nm}^{-1}] < 0.80$. Hence, by choosing suitable set of different optical conditions, SANS-U covers a wide q-range of $0.04 < q[\mathrm{nm}^{-1}] < 3.5$ in the case of $\lambda = 0.70$ nm.

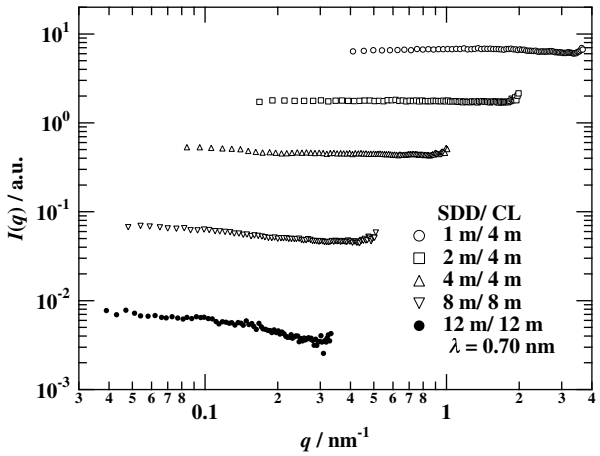

FIG. 9: Background corrected scattering profiles of a polyethylene slab (3 mm thick), indicating the accessible q-ranges at various optical conditions.

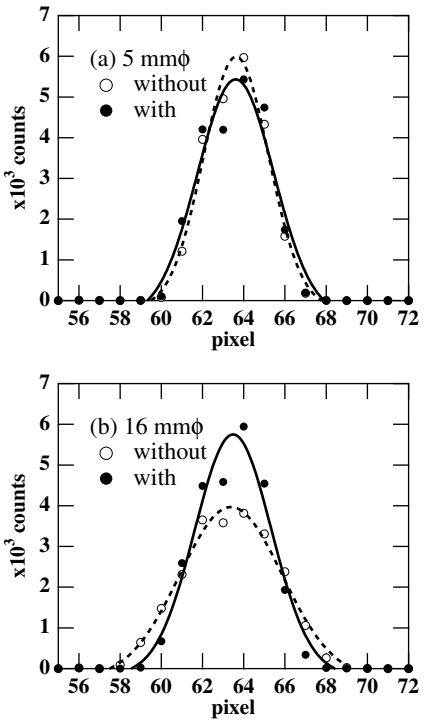

FIG. 10: The center beam profiles with (filled symbols with solid line) and without the focusing collimation (open symbols with dashed line) system. (a) 5 mm and (b) 16mm sample apertures in diameter.

F. Focusing collimation

The performance of the focusing collimation with the material lenses was examined. In the upgraded

SANS-U, a beam guide with 54 biconcave lenses can be mounted by remote control from the SANS-U control panel. Here, the specification of the lens is as follows; the curvature radius = 25.0 mm, the center thickness = 1.00 mm, and the outer diameter = 30.0 mm. In the case of SDD = 8 m symmetric optical arrangement with 20 mmϕ sample aperture, the transmittance of a $\lambda = 0.7$ nm neutron beam was 0.51 and the focal spot size on the detector plane was calculated to be 9.5 mm in diameter. Figure 10 shows the comparisons of the incident beam profiles at the detector plane with and without the focusing collimation system for the beam sizes of (a) 5 mmϕ and (b) 16 mmϕ. By enlarging the sample aperture, both the peak intensity and the sharpness of the profile was improved by the factors of 1.4 and 1.3 times, respectively. Hence, it is recommended to employ this setup if a large sample is available.

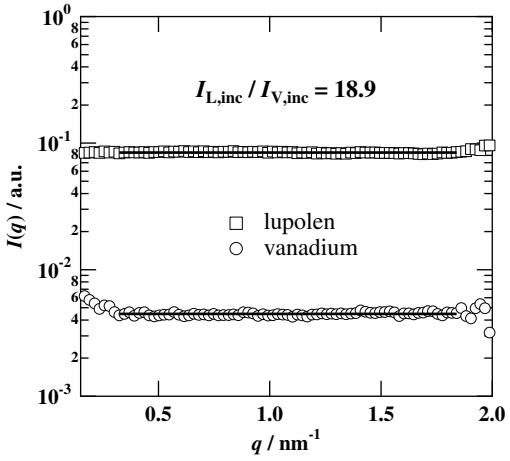

FIG. 11: Comparison of the incoherent scattering intensities from vanadium and a polyethylene slab (3 mm in thick).

IV. DATA TREATMENT AT THE SANS-U

A. Absolute intensity calibration

One of the greatest advantages of the SANS technique is that the absolute scattering intensity is easily obtained by scaling the observed scattering intensity with a standard sample, e.g., a vanadium standard or water. Since the zero-q scattering intensity, $I(q = 0)$, contains useful information such as molecular weight of polymers and the association number of particles, it is recommended to obtain the absolute scattering intensity at the SANS-U. Because of weak scattering and difficulty in handling of vanadium, vanadium-calibrated materials are used as the secondary standard samples. The secondary standard for absolute intensity calibration is Lupolen (polyethylene (PE) slab) at SANS-U. The following fact should be noted here. A PE slab with known mass density is more suitable as a standard than water since the latter contains larger inelastic scattering and is more difficult to distinguish incoherent scattering from inelastic scattering (Sears, 1992). The effect of multiple scattering from PE slabs has been properly taken into consideration (Shibayama, 2005). A calibrations for Lupolen was carried out by scaling the incoherent scattering intensity with that from the primary standard, vanadium.

In the case of single scattering, the normalized scattering intensity, $\mu(q)$ [-] is expressed by the following equation (Wignall, 1987).

$$\mu_i(q) \equiv \frac{I_i(q)}{\Phi_0 \epsilon A \Delta\Omega} = T_i t_i \left(\frac{\mathrm{d}\Sigma}{\mathrm{d}\Omega}\right)_i (q) \qquad (2)$$

where $I_i(q)$ [s^{-1}], T_i[$-$], and t_i[cm] are the corrected scattering intensity, the transmission for neutrons, and the thickness of i (i = L, V or S for Lupolen, vanadium or another sample). Φ_0[cm$^{-2}s^{-1}$] is the flux of the incident beam, ϵ[$-$] is the efficiency of the detector, A[cm^2] is the irradiated cross section of the sample, $\Delta\Omega$[sr] is the solid angle at the detector plane. $I_i(q)$[s^{-1}] is given by

$$I_i(q) = \frac{\left[I_i^0(q) - I_{\mathrm{bg}}^0(q)\right] - T_i\left[I_{\mathrm{c}}^0(q) - I_{\mathrm{bg}}^0(q)\right]}{\cos^3 2\theta} \qquad (3)$$

where $I_i^0(q)$ [s^{-1}] is the count rate of the scattered neutrons from the sample (in a cell), $I_{\mathrm{bg}}^0(q)$[s^{-1}] is the detector dark current, $I_{\mathrm{c}}^0(q)$[s^{-1}] is the air scattering (or the scattering from the sample cell). The factor $1/\cos^3 2\theta$ corresponds to the correction for the oblique incidence and the q-dependence of the solid angle necessary for high-q region. By employing an identical optical condition for each measurement, i.e., the sample and the standard, we obtain a simple equation,

$$\mu_{\mathrm{L}} = T_{\mathrm{V}} t_{\mathrm{V}} \left(\frac{\mathrm{d}\Sigma}{\mathrm{d}\Omega}\right)_{\mathrm{V}} \frac{I_{\mathrm{L,inc}}}{I_{\mathrm{V,inc}}} \qquad (4)$$

where T_{V} and t_{V} are the transmission and the thickness of the vanadium, and $I_{\mathrm{L,inc}}$ and $I_{\mathrm{V,inc}}$ are the corrected scattering intensities of Lupolen and the vanadium. Note that $I_{\mathrm{L,inc}}$, $I_{\mathrm{V,inc}}$ and therefore μ_{L} are q-independent because both Lupolen and the vanadium show incoherent scattering in small-angle region. The differential scattering cross section of vanadium, $(\mathrm{d}\Sigma/\mathrm{d}\Omega)_{\mathrm{V}}$, is estimated with the following equation,

$$\left(\frac{\mathrm{d}\Sigma}{\mathrm{d}\Omega}\right)_{\mathrm{V}} = \frac{\rho_{\mathrm{V}} \sigma_{\mathrm{V,inc}}}{4\pi} \qquad (5)$$

where $\sigma_{\mathrm{V,inc}}$ is the incoherent scattering cross section, $\rho_{\mathrm{V}} = d_{\mathrm{V}} N_{\mathrm{A}}/M_{\mathrm{V}}$ and d_{V} are the number and the mass density, N_{A} is Avogadro's number and M_{V} is the molecular mass of vanadium. These values are well known from literatures as $\sigma_{\mathrm{V,inc}} = 5.08 \times 10^{-24}\mathrm{cm}^2, d_{\mathrm{V}} = 5.8\mathrm{gcm}^{-3}, M_{\mathrm{V}} = 50.94$. Therefore, $(\mathrm{d}\Sigma/\mathrm{d}\Omega)_{\mathrm{V}} = 0.0278\mathrm{cm}^{-1}$.

The corrected profiles, $I_{\mathrm{L,inc}}$ and $I_{\mathrm{V,inc}}$ are shown in Figure 11. The ratio $I_{\mathrm{L,inc}}/I_{\mathrm{V,inc}}$ was evaluated to be 18.9. By substituting this value and the values

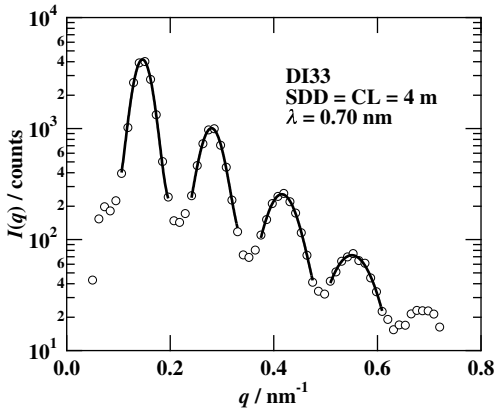

FIG. 12: The scattering intensity from DI33. The solid lines indicate the fits of the scattering peaks with Gaussian functions, which allow an estimation of a decay of q-resolution with q.

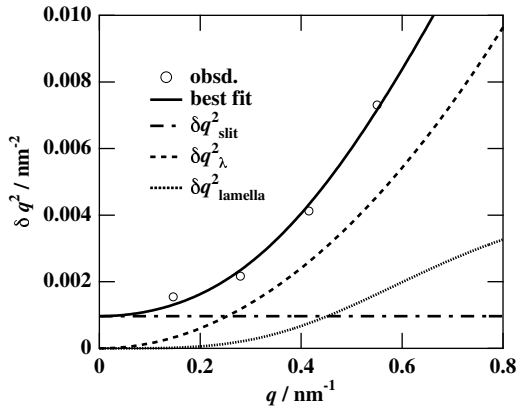

FIG. 13: The q-dependence of FWHMs of the Bragg reflections from DI33.

$T_{\rm vanadium}$ and $t_{\rm vanadium}$, $\mu_{\rm L} = 7.45 \times 10^{-2}$ was obtained from Eq. 3. Note that the value $\mu_{\rm L} = 7.45 \times 10^{-2}$ is a material constant of Lupolen.

In practice, the differential scattering cross section of a sample, $(\mathrm{d}\Sigma/\mathrm{d}\Omega)_{\rm S}(q)$, is obtained by the following equation.

$$\left(\frac{\mathrm{d}\Sigma}{\mathrm{d}\Omega}\right)_{\rm S}(q) = \frac{I_{\rm S}(q)}{I_{\rm L,inc}} \frac{\mu_{\rm L}}{T_{\rm S} t_{\rm S}} \tag{6}$$

B. q-resolution

Next, let us discuss the q-resolution of this instrument. The q-resolution was evaluated with the sharpness of the Bragg reflections from the DI33 sample with SDD = CL = 4 m and $\lambda = 0.70$ nm (Figure 12). The relative peak positions obey the lamellar stacking, i.e., 1:2:3:... The square of FWHM of the peaks, δq^2, is plotted against q (Figure 13). It is clearly shown that FWHM becomes larger with increasing q. Smearing occurs by the following contributions; (i) an aperture smearing due to a finite size of the incident beam, (ii) the wavelength distribution of the incident neutrons, and (iii) the paracrystal nature of the microdomains in block copolymers (Hosemann, 1962). The instrumental smearing, $\delta q_{\rm inst}$, is obtained by the sum of (i) and (ii), and is evaluated by

$$q = \frac{4\pi}{\lambda}\sin\theta \approx \frac{4\pi}{\lambda}\theta(\mathrm{whensmall-angle}) \tag{7}$$

$$\delta q^2_{\rm inst} = \delta q^2_{\lambda} + \delta q^2_{\rm apert} \tag{8}$$

$$\delta q^2_{\lambda} = \left|\frac{\partial q}{\partial \lambda}\delta\lambda\right| = \left|-\frac{4\pi}{\lambda^2}\sin\theta\delta\lambda\right| = \left|-q\frac{\delta\lambda}{\lambda}\right| \propto q^2 \tag{9}$$

$$\delta q^2_{\rm apert} = \left|\frac{\partial q}{\partial \theta}\delta\theta\right| \tag{10}$$

where the wavelength $\lambda = 0.70$ nm and its resolution $\delta\lambda/\lambda = 0.10$ (FWHM). The contribution (i) can be estimated from the optical arrangement. From Figure 6, the square of FWHM of the center beam profile at the detector plane, $\delta q^2_{\rm apert}$, was evaluated to be $1.60 \times 10^{-3}\mathrm{nm}^{-2}$. $\delta q^2_{\rm apert}$ is also evaluated by the following equation (Mildner, 1984; Glinka, 1998),

$$\delta q^2_{\rm apert} = \frac{8\ln 2(2\pi)^2}{12\lambda^2}\left[3\frac{R_1^2}{L_1^2} + 3\frac{R_2^2}{L'^2} + \frac{(\Delta R)^2}{L_2^2}\right] \tag{11}$$

where R_1 and R_2 are the radii of the source and sample apertures, ΔR is the detector resolution (FWHM), and L_1 and L_2 are the incident and scattered flight path lengths, and L' is the reduced path length, $L' = L_1L_2/(L_1+L_2)$, respectively. According to Eq. (9), on the other hand, δq^2_{λ} is proportional to q^2, meaning that the q-resolution becomes worse by increasing q. In order to estimate the smearing effect of paracrystal nature of the sample, $\delta q^2_{\rm lam}$, we adopted the paracrystal theory (Hosemann, 1962; Shibayama 1986). The theory gives

$$\delta q^2_{\rm lam} = \frac{4\ln 2}{\pi}\frac{\left\{1-\exp\left[-2\pi^2 g^2 (q/q_1)^2\right]\right\}^2}{4q_1^2} \tag{12}$$

where g is the Hosemann ' s g-factor, q_1 the first peak position of Bragg reflection, and d the Bragg spacing of the lamellar structure. Thus the square of the total FWHM of the scattering peaks for the paracrystal system is

$$\begin{aligned}\delta q^2 &= \delta q^2_{\rm apert} + \delta q^2_{\lambda} + \delta q^2_{\rm lam} \\ &= \delta q^2_{\rm apert} + \left(\frac{\delta\lambda}{\lambda}\right)^2 q^2 \\ &+ \frac{4\ln 2}{\pi}\frac{\left\{1-\exp\left[-2\pi^2 g^2 (q/q_1)^2\right]\right\}^2}{4q_1^2}\end{aligned} \tag{13}$$

Curve fitting was carried out on the plot of δq^2 vs q by floating parameters $\delta q^2_{\rm apert}$, $\delta\lambda/\lambda$, and g. The fitted values are in good agreement with obtained with other methods (Table 1) and we can conclude that the instrumental smearing effect in high q region is dominated by the λ-distribution.

TABLE I: Comparison between values for the q-resolution function from the experiment, calculation and the fitting. (a) From the center beam profile on the detector, (b) (Mildner, 1984; Glinka, 1998), (c) From the catalogue from the manufacturer, (d) (Shibayama, 1986)

	exp.	calc.	fit
$\Delta q_{\rm apert}[{\rm nm}^{-2}]$	$0.00160^{\rm (a)}$	$0.000763^{\rm (b)}$	0.000967
$\Delta\lambda/\lambda$(FWHM)	n/a	$0.1^{\rm (c)}$	0.123
g	$0.05^{\rm (d)}$	n/a	0.0559

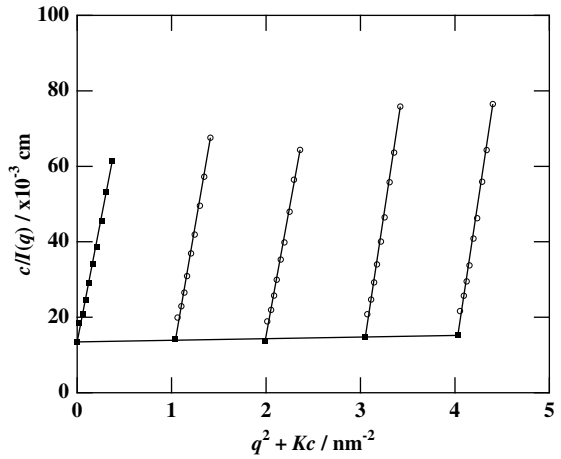

FIG. 14: The Zimm plot of PS / cyclohexane solutions measured at 310 K. Here, $K = 1$ nm^{-2} g^{-1} ml is a constant.

C. Experimental Example

In order to demonstrate the performance of SANS-U, the molecular weight of a standard polystyrene (PS, the number and weight average molecular weights being $M_{\rm n} = 2.08 \times 10^4$ and $M_{\rm w} = 2.22 \times 10^4$, respectively, the polydispersity index = 1.07; Polymer Source Inc., Doval, Monteral, Canada). Deuterated cyclohexane solutions of the PS were prepared, and SANS experiments were carried out at 310 K (Siporska, 2003). The SANS data were analyzed with the Zimm equation given by

$$\frac{(b_1 v_0/v_1 - b_1)^2 N_{\rm A} c}{I(q) m^2} = \frac{1}{M_{\rm w}} \left[1 + \frac{1}{3} R_{\rm g}^2 q^2 + ...\right] + 2A_2 c \tag{14}$$

where b_i and v_i are segment length and the molar volume of the polymer segment (i = P) and the solvent (i = S), $N_{\rm A}$ is the Avogadro number, m is the monomer molecular weight of the polymer, A_2 is the second virial coefficient, $R_{\rm g}$ is the radius of gyration, and c is the polymer concentration. Figure 14 shows the Zimm plot of the PS solutions. By extrapolating the data to $c = 0$ and $q = 0$, we obtained $M_{\rm w} = 2.10 \times 10^4$, which is in good agreement with the catalogue value by the supplier. The radius of gyration of the PS chains, $R_{\rm g}$, were evaluated to be 3.89 nm, which is in accordance with the calculated value (4.02 nm) from the molecular weight with the following equation (Cotton, 1974; Melnichenko, 1998),

$$R_g = 0.027 M_{\rm w}^{1/2} [{\rm nm}] \tag{15}$$

V. CONCLUSION

The SANS-U instrument was upgraded and the new performance was evaluated. (1) The new multi-wired area detector with a new data-acquisition system was installed, enlarging the dynamic range of neutron counting with higher reliability. (2) The new control system, i.e., LabVIEW-based PC system, is a user-friendly interface with versatile possible-modifications compared with the old VAX-sequencer system. (3) An in-situ real-time circular averaging allows prompt evaluation of the experiment. The method of the absolute intensity calibration used at SANS-U was confirmed by calibration of the standard samples with vanadium and water. (4) A focusing collimation system was installed. This system is advantageous for investigation of large samples than 10 mmϕ because of larger neutron flux without loosing the resolution. (5) The performance of the upgraded SANS-U was examined by studying the molecular weight and the radius of gyration for a standard polystyrene sample. The new SANS-U will serve a powerful SANS instrument for scientists from overseas as well as domestic users.

[1] Choi, S.-M., Barker, J. G., Glinka, C. J., Cheng, Y. T. & Gammel, P. L. (2000) *J. Appl. Cryst.* **33**, 793–796.

[2] Cotton, J. P., Decker, D., Benoit, H., Farnoux, B., Higgins, J. S., Jannink, G., Ober, R., Picot, C. & des Cloizeaux, J. (1974) *Macromolecules* **7**, 863.

[3] Eskildsen, M. R., Gammel, P. L., Isaacs, E. D., Detlefs, C., Mortensen, K., & Bishop, D. J. (1998) *Nature* **391**, 563–566.

[4] Friedrich, H., Wagner, V. & Wille, P. (1989) *Physica B* **156 & 157**, 547–549.

[5] Glinka, C. J., Barker, J. G., Hammouda, B., Krueger, S., Moyer, J. J. & Orts, W. (1998) *J. Appl. Cryst.* **31**, 430–445.

[6] Heenan, R. K., Penfold, J. & King, S. M. (1997) *J. Appl. Cryst.* **30**, 1140–1147.

[7] Higgins, J. S. & Benoit, H. C (1994) *Polymers and Neutron Scattering*, Clarendon Press, Oxford.

[8] Hosemann, R. & Bagchi, S. N. (1962) *Direct Analysis*

of Diffraction by Matter, North-Holland: Amsterdam.
[9] Ito, Y., Imai, M. & Takahashi, S. (1995) *Physica B* **213 & 214**, 889–891.
[10] Matsuhita, Y. (1995) *private communication.*
[11] Melnichenko, Y. B., Wignall, G. D., Van Hook, A. W., Szydlowski, J., Wilczura, H. & Rebelo, L. P. (1998) *Macromolecules* **31**, 8436–8438.
[12] Mildner, D. F. & Carpenter, J. M. (1984) *J. Appl. Cryst.* **17**, 249–256.
[13] Nasimova, I. R., Karino, T., Okabe, S., Nagao, M. & Shibayama, M. (2004) *J. Chem. Phys.* **121**, 9708–9715.
[14] Nasimova, I. R., Karino, T., Okabe, S., Nagao, M. & Shibayama, M. (2004) *Macromolecules* **37**, 8721–8729.
[15] Noda, Y., Utiki, T. & Kajitani, M. (1983) *J. Cryst. Soc. of Jpn.* **25**, 222–227.
[16] Otomo, T., Furusaka, M., Satoh, S., Itoh, S., Adachi, T., Shimizu, S. & Takeda, M. (1999) *J. Phys. Chem. Sol.* **60**, 1579–1582.
[17] Schelten, J., Wignall, G. D. & Ballard, D. G. H. (1974) *Polymer* **15**, 682–685.
[18] Sears, V. F. (1992) *Neutron News* **3**, 29–37.
[19] Shibayama, M. & Hashimoto, T. (1986) *Macromolecules* **19**, 740–749.
[20] Shibayama, M., Isono, K., Okabe, S., Karino, T. & Nagao, M. (2004) *Macromolecules* **37**, 2909–2918.
[21] Shibayama, M., Nagao, M., Okabe, S. & Karino, T., *J. Phy. Soc. Jpn.*, **74**, 2728–2736.
[22] Siporska, A., Szydlowski, J. & Rebelo, L. P. N. (2003) *Phys. Chem. Chem. Phys.* **5**, 2996–3002.
[23] Takahashi, Y., Noda, M., Naruse, M., Kanaya, T., Watanabe, H., Kato, T., Imai, M. & Matsushita, Y. (2000) *J. Soc. Rheol. Jpn.* **28**, 187–191.
[24] Wignall, G. D. & Bates, F. S. (1987) *J. Appl. Cryst.* **20**, 28–40.